2013

Surface plasmon-enhanced transverse magnetic second-harmonic generation

Wei Zheng
Wiliam & Mary

Aubrey T. Hanbicki

Berry T. Jonker

Gunter Lupke
William & Mary, gxluep@wm.edu

Recommended Citation

Zheng, Wei; Hanbicki, Aubrey T.; Jonker, Berry T.; and Lupke, Gunter, Surface plasmon-enhanced transverse magnetic second-harmonic generation (2013). *Optics Express*, 21(23), 28842-28848. 10.1364/OE.21.028842

Surface plasmon-enhanced transverse magnetic second-harmonic generation

Wei Zheng,[1,*] Aubrey T. Hanbicki,[2] Berry T. Jonker,[2] and Gunter Lüpke[1]

[1]*Department of Applied Science, College of William & Mary, Williamsburg, VA 23187, USA*
[2]*Materials Science & Technology Division, Naval Research Laboratory, Washington, D.C. 20375, USA*
[*]*wzheng@email.wm.edu*

Abstract: We present experimental studies on surface plasmon (SP) enhanced transverse magnetic second-harmonic generation (T-MSHG) in single-crystal iron films grown by molecular beam epitaxy at room temperature on MgO (001) substrates. We show that it is possible to achieve both strongly enhanced T-MSHG intensity and high magnetic contrast ratio under attenuated total reflection configuration without using complex heterostructures because MSHG is generated directly at the iron surface where SPs are present. The T-MSHG has a much larger contrast ratio than transverse magneto-optical Kerr effect (T-MOKE) and shows great potential for a new generation of bio-chemical sensors due to its very high surface sensitivity. In addition, by analyzing the experimental results and the simulations based on SP field-enhancement theory, we demonstrate that the second-order susceptibility of MSHG shows great anisotropy and the tensor χ_{xzz}^{odd} is dominant in our sample.

OCIS codes: (190.2620) Harmonic generation and mixing; (190.4350) Nonlinear optics at surfaces; (240.6680) Surface plasmons; (160.3820) Magneto-optical materials; (230.3810) Magneto-optic systems.

References and links

1. H. Raether, "Surface plasmons on smooth and rough surfaces and on gratings," in *Tracts in Modern Physics* (Springer-Verlag, 1988, Vol. 111).
2. H. J. Simon, D. E. Mitchell, and J. G. Watson, "Optical second-harmonic generation with surface plasmons in silver films," Phys. Rev. Lett. **33**(26), 1531–1534 (1974).
3. S. Palomba and L. Novotny, "Nonlinear excitation of surface plasmon polaritons by four-wave mixing," Phys. Rev. Lett. **101**(5), 056802 (2008).
4. V. I. Safarov, V. A. Kosobukin, C. Hermann, G. Lampel, J. Peretti, and C. Marlière, "Magneto-optical effects enhanced by surface plasmons in metallic multilayer films," Phys. Rev. Lett. **73**(26), 3584–3587 (1994).
5. B. Sepúlveda, A. Calle, L. M. Lechuga, and G. Armelles, "Highly sensitive detection of biomolecules with the magneto-optic surface-plasmon-resonance sensor," Opt. Lett. **31**(8), 1085–1087 (2006).
6. D. Regatos, D. Fariña, A. Calle, A. Cebollada, B. Sepúlveda, G. Armelles, and L. M. Lechuga, "Au/Fe/Au multilayer transducers for magneto-optic surface plasmon resonance sensing," J. Appl. Phys. **108**(5), 054502 (2010).
7. V. V. Temnov, G. Armelles, U. Woggon, D. Guzatov, A. Cebollada, A. Garcia-Martin, J. Garcia-Martin, T. Thomays, A. Leitenstorfers, and R. Bratschitschs, "Active magneto-plasmonics in hybrid metal–ferromagnet structures," Nat. Photonics **4**(2), 107–110 (2010).
8. A. V. Chetvertukhin, A. A. Grunin, A. V. Baryshev, T. V. Dolgova, H. Uchida, M. Inoue, and A. A. Fedyanin, "Magneto-optical Kerr effect enhancement at the Wood's anomaly in magnetoplasmonic crystals," J. Magn. Magn. Mater. **324**(21), 3516–3518 (2012).
9. N. Bonod, R. Reinisch, E. Popov, and M. Nevière, "Optimization of surface-plasmon-enhanced magneto-optical effects," J. Opt. Soc. Am. B **21**(4), 791–797 (2004).
10. Y. Demidenko, D. Makarov, O. G. Schmidt, and V. Lozovski, "Surface plasmon-induced enhancement of the magneto-optical Kerr effect in magnetoplasmonic heterostructures," J. Opt. Soc. Am. B **28**(9), 2115–2122 (2011).
11. Y. R. Shen, *The Principles of Nonlinear Optics* (Wiley, 1984).
12. A. Kirilyuk and T. Rasing, "Magnetization-induced second harmonic generation," in *Handbook of Magnetism and Advanced Magnetic Materials*, Volume 3: Novel Techniques for Characterizing and Preparing Samples (John Wiley & Sons, Ltd. 2007).

#197522 - $15.00 USD Received 17 Sep 2013; revised 8 Oct 2013; accepted 8 Oct 2013; published 15 Nov 2013

13. M. Fiebig, D. Fröhlich, B. B. Krichevtsov, and R. V. Pisarev, "Second harmonic generation and magnetic-dipole-electric-dipole interference in antiferromagnetic Cr_2O_3," Phys. Rev. Lett. **73**(15), 2127–2130 (1994).
14. G. Tessier, C. Malouin, P. Georges, A. Brun, D. Renard, V. V. Pavlov, P. Meyer, J. Ferré, and P. Beauvillain, "Magnetization-induced second-harmonic generation enhanced by surface plasmons in ultrathin Au/Co/Au metallic films," Appl. Phys. B **68**(3), 545–548 (1999).
15. D. M. Newman, M. L. Wears, R. J. Matelon, and D. Mchugh, "Non-linear optics and magneto-optics on nano-structured interfaces," Appl. Phys. B **74**(7-8), 719–722 (2002).
16. V. K. Valev, A. V. Silhanek, W. Gillijns, Y. Jeyaram, H. Paddubrouskaya, A. Volodin, C. G. Biris, N. C. Panoiu, B. De Clercq, M. Ameloot, O. A. Aktsipetrov, V. V. Moshchalkov, and T. Verbiest, "Plasmons reveal the direction of magnetization in nickel nanostructures," ACS Nano **5**(1), 91–96 (2011).
17. Y. Fan, K. J. Smith, G. Lüpke, A. T. Hanbicki, R. Goswami, C. H. Li, H. B. Zhao, and B. T. Jonker, "Exchange bias of the interface spin system at the Fe/MgO interface," Nat. Nanotechnol. **8**(6), 438–444 (2013).
18. W. H. Weber and G. W. Ford, "Optical electric-field enhancement at a metal surface arising from surface-plasmon excitation," Opt. Lett. **6**(3), 122–124 (1981).
19. P. Berini, "Long-range surface plasmon polaritons," Advances in Optics and Photonics **1**(3), 484–588 (2009).
20. G. J. Kovacs, "Surface polariton in the ATR angular spectra of a thin iron film bounded by dielectric layers," J. Opt. Soc. Am. **68**(10), 1325–1332 (1978).
21. K. Aslan, M. Weisenberg, E. Hortle, and C. D. Geddes, "Surface plasmon coupled chemiluminescence from iron thin films: directional and approaching fixed angle observation," J. Appl. Phys. **106**(1), 014131 (2009).
22. T. Y. F. Tsang, "Surface-plasmon-enhanced third-harmonic generation in thin silver films," Opt. Lett. **21**(4), 245–247 (1996).
23. M. A. Ordal, L. L. Long, R. J. Bell, S. E. Bell, R. R. Bell, R. W. Alexander, Jr., and C. A. Ward, "Optical properties of the metals Al, Co, Cu, Au, Fe, Pb, Ni, Pd, Pt, Ag, Ti, and W in the infrared and far infrared," Appl. Opt. **22**(7), 1099–20 (1983).

1. Introduction

Surface plasmons (SPs) are electromagnetic waves that propagate along metal-dielectric interfaces. One of their most important features is a strong enhancement of the electromagnetic field at the metal-dielectric interface with the excitation of SPs by light [1]. This field enhancement has many applications including enhanced harmonic generation [2,3] and an enhanced magneto-optical Kerr effect (MOKE) [4]. The interaction between SPs and magneto-optical effects has also generated much interest because of the potential for applications in bio-chemical sensors [5,6] and the magnetic control/modulation of SPs [7].

MOKE changes the polarization of incoming light when interacting with magnetic media, and in general, it is typical to use a thick magnetic layer to obtain a large change of polarization because MOKE is a bulk effect. High losses in magnetic layers cause an over damping of plasmon resonance, however and thus impairs SP enhancement effects on MOKE. To achieve a balance between high quality SPs and a respectable MOKE signal, a number of experimental and theoretical studies have been carried out to optimize the magnetic multilayer structures [8–10] and noble metal/ferromagnetic/noble metal heterostructures have become the prevailing configuration.

A more surface sensitive magneto-optic effect is magnetic second-harmonic generation (MSHG). This effect is sensitive to the interface or surface magnetization where the symmetry is broken [11,12]. Compared to metal surface second-harmonic generation (SHG), MSHG contains nonzero magnetic components of the second-order nonlinear susceptibility tensor which makes MSHG extremely sensitive to subtle modifications of the spin-polarized electronic structure of transition metal surfaces [13], the same region where SPs are present. This is a very active area of research and, for example, Tessier et al. reported the reversal of MSHG contrast by SPs generated from a standard Au/Co/Au heterostructure [14], the enhanced MSHG signal by SPs on nickel gratings has been observed by Newman et al. [15], and Valve et al showed that surface plasmon contributions to the MSHG signal can reveal the direction of the magnetization of Nickel nanostructures [16].

In this paper, we present a study on SP-enhanced MSHG from single-crystal iron film samples under the Kretschmann-Raether configuration [1]. Large enhancement of both the MSHG signal intensity and magnetic contrast ratios [12] are observed under attenuated total reflection (ATR). In contrast to MOKE, MSHG is a nonlinear magneto-optical effect, whose

#197522 - $15.00 USD Received 17 Sep 2013; revised 8 Oct 2013; accepted 8 Oct 2013; published 15 Nov 2013

inherent surface sensitivity suggests that it would be ideally paired with SPs for sensing applications.

2. Transverse MSHG and experimental setup

In the electric-dipole approximation, for crystals with a magnetization M induced by spontaneous or magnetic field, the second-order nonlinear optical polarization can be written as [11,12]:

$$P^{nl}(2\omega) = \varepsilon_0 \chi^{cr} E(\omega)E(\omega) \pm \varepsilon_0 \chi^{magn}(\pm M)E(\omega)E(\omega), \quad (1)$$

where the first term describes the non-magnetic contribution while the second one describes MSHG, which exists only in the presence of M. χ^{cr} and χ^{magn} are non-intermixing tensors for crystallographic and magnetization contributions, respectively, ε_0 is the electric constant, E is the fundamental field, and ω is the fundamental frequency. The total (MSHG) signal is thus given by

$$I^{2\omega} = \left(P^{nl}(2\omega)\right)^2, \quad (2)$$

and the magnetic contrast or asymmetry is defined by:

$$A = \frac{I^{2\omega}(+M) - I^{2\omega}(-M)}{I^{2\omega}(+M) + I^{2\omega}(-M)}, \quad (3)$$

where $I^{2\omega}(+M)$ and $I^{2\omega}(-M)$ represent the signal intensity under opposite magnetization directions [12,14].

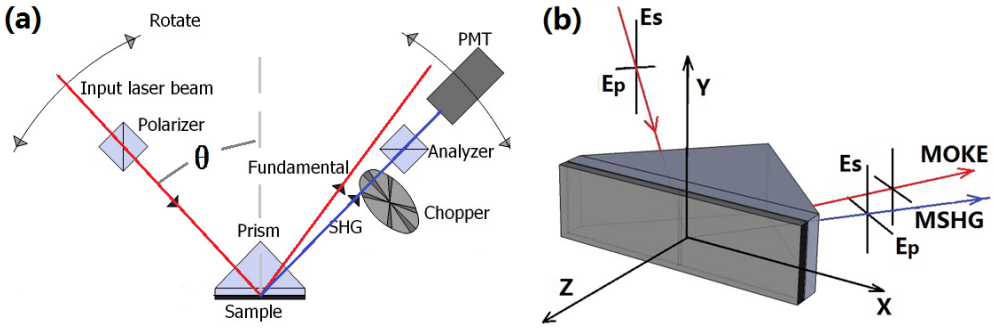

Fig. 1. (a) Experimental setup and (b) coordinate system.

Figure 1(a) depicts our experimental setup. In our configuration θ is the incident angle, a photomultiplier tube (PMT) is used to detect the MSHG signal, and a photo diode is used to record the MOKE signal. Figure 1(b) defines the coordinate system, beam geometry and sample surface. A P-polarized picosecond pulsed beam from a Ti:Sapphire laser system is used as the source for MSHG, MOKE, and SPs. The external magnetic field (H) is applied along the y-axis (transverse geometry). The Kretschmann-Raether configuration [1] is used to excite SPs.

For light incident in the x-z plane [Fig. 1(b)], the longitudinal, transverse, and polar MSHG are classified according to the direction of magnetization component parallel to the x, y, and z-axis, respectively. In this study, the external magnetic field is applied along the y-axis, so the transverse (T) MSHG is studied. The nonlinear susceptibility tensors for T-MSHG are [12]

#197522 - $15.00 USD Received 17 Sep 2013; revised 8 Oct 2013; accepted 8 Oct 2013; published 15 Nov 2013

$$\chi_{ijk}^{(T)}=\begin{bmatrix}\chi_{xxx}^{odd} & \chi_{xyy}^{odd} & \chi_{xzz}^{odd} & 0 & \chi_{xzx}^{even} & 0\\ 0 & 0 & 0 & \chi_{yzy}^{even} & 0 & \chi_{yxy}^{odd}\\ \chi_{zxx}^{even} & \chi_{zyy}^{even} & \chi_{zzz}^{even} & 0 & \chi_{zxz}^{odd} & 0\end{bmatrix}, \tag{4}$$

where the odd terms change sign with magnetization reversal and determine the magnetic contrast and switching process, while the even terms are not sensitive to the magnetization but are still needed for the magnetic contrast. For T-MSHG with P-polarized fundamental fields, the second-order nonlinear optical polarization is calculated as:

$$\begin{bmatrix}P_x\\P_y\\P_z\end{bmatrix}^{(T)}=\varepsilon_0\cdot\chi_{ijk}^{(T)}\cdot\begin{pmatrix}E_x^2\\0\\E_z^2\\0\\2E_xE_z\\0\end{pmatrix}=\varepsilon_0\cdot\begin{bmatrix}\chi_{xxx}^{odd}\cdot E_x^2+\chi_{xzz}^{odd}\cdot E_z^2+\chi_{xzx}^{even}\cdot 2E_zE_x\\0\\\chi_{zxx}^{even}\cdot E_x^2+\chi_{zzz}^{even}\cdot E_z^2+\chi_{zxz}^{odd}\cdot 2E_zE_x\end{bmatrix}. \tag{5}$$

Note that the expression of polarization for longitudinal (L) MSHG includes odd terms only in $P_y^{(L)}$ [12]. Therefore, the analyzer is set to P-polarization to screen out the contribution of L-MSHG signal.

3. Experimental results

Under the Kretschmann-Raether configuration and with a P-polarized incident beam, the reflection is maximized when the total reflection condition is reached. The reflection decreases sharply when the incident angle increases further, which is called attenuated total reflection (ATR). The ATR can be explained by either destructive interference or coupling of light energy into the SPs on the metal surface [1]. The intensity of the electro-magnetic field on the metal surface at the metal-air interface becomes enhanced under the ATR condition, and reaches its maximum at the bottom of the ATR curve for noble metals.

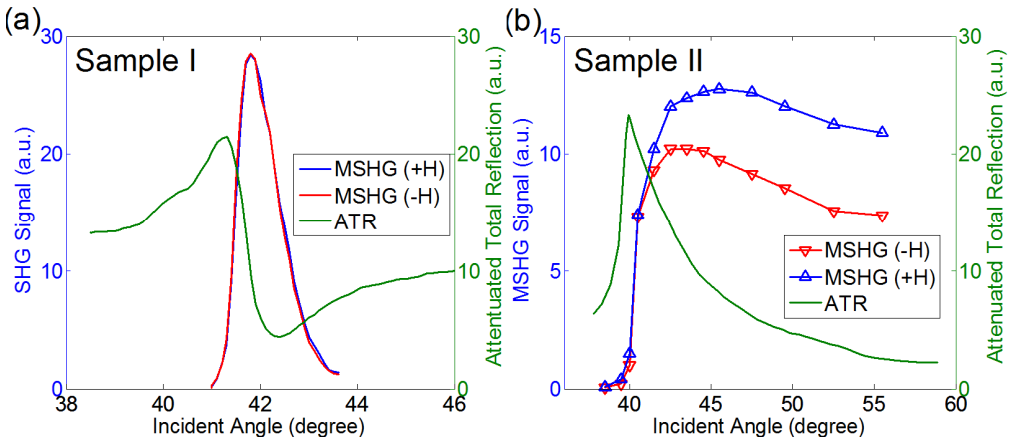

Fig. 2. (a) MSHG signal from sample I with large SPs enhancement but no apparent magnetic contrast; (b) Sample II with large SPs enhancement and huge magnetic contrast.

Sample I is a 10-nm thick single crystal Fe film grown on an MgO (001) substrate with axis [110] along the x-direction [17], capped with a 40-nm thick Au layer. This structure is expected to have huge field enhancement due to the Au cap layer. A very large MSHG signal is generated under ATR condition because of the enhancement of the fundamental field [Fig. 2(a)]. The magnetic contrast (Eq. (3)) in the MSHG signal is negligible when a magnetic field

#197522 - $15.00 USD Received 17 Sep 2013; revised 8 Oct 2013; accepted 8 Oct 2013; published 15 Nov 2013

of H = +/– 100 Oe is applied along the y-direction. This result provides some important information: First, the experiment confirms that the enhanced MSHG signal under ATR condition is generated at the Au surface (Au/air interface) [2,18] and not the Fe/Au interface because there is no magnetic response. Second, it shows that the MSHG response from the Fe-MgO interface is negligible under this configuration.

Of more interest is Sample II, which is also a 10-nm thick single-crystal Fe film grown on an MgO (001) substrate with axis [110] along the x direction, but without a Au cap layer. This structure is expected to exhibit large SPs-enhanced magnetic response from the Fe surface (Fe/air interface). One common concern is that the Fe film is not suitable for huge field enhancement due to its large damping of electromagnetic fields compared to noble metals like Ag and Au. Actually, Fe films have been widely studied in surface plasmon coupled emission (SPCE), plasmon coupled chemi-luminescence, and long-range surface polaritons (LRSPs) by the ATR method [19–21]. Furthermore, as mentioned in the introduction section, other pure magnetic materials alone have been used to study the interaction between MSHG and SPs [15,16].

Figure 2(b) shows the angle-of-incidence dependent T-MSHG signal from sample II for applied magnetic fields H = +/– 100 Oe. Note that the ATR curve is not as sharp as that of sample I [Fig. 2(a)] as it is stretched out due to absorption, i.e. strong damping. Without ATR [$\theta < 40°$, where θ is the incident angle, as defined in Fig. 1(a)], the MSHG signal is very small and the magnetic contrast is negligible. Under ATR condition with generation of SPs leading to an enhanced surface field, both the MSHG signal strength and the contrast ratio become enhanced. As a result, a very strong signal with good magnetic contrast is observed. This is the SP-enhanced T-MSHG effect.

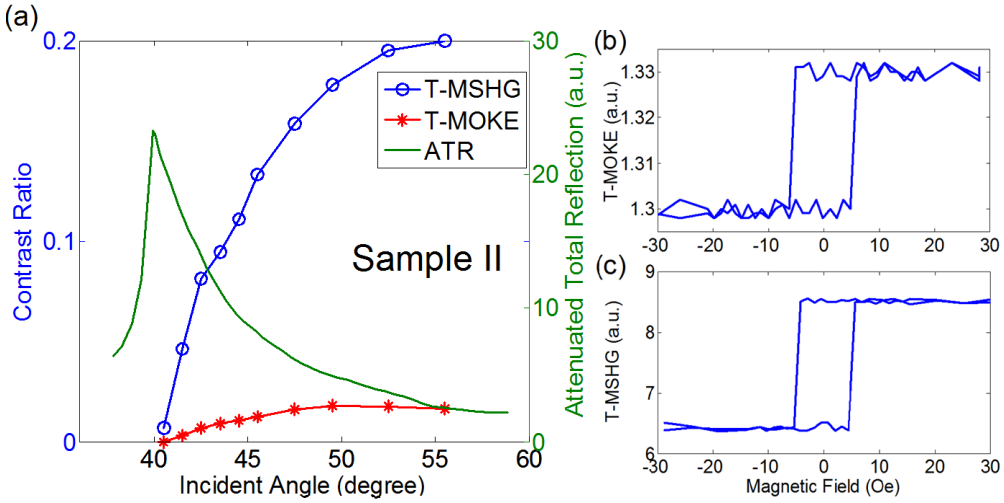

Fig. 3. (a) Contrast ratio of T-MSHG and T-MOKE under ATR condition; (b) and (c) hysteresis loops obtained when the incident angle is 45.6° for P-polarized light-in and P-polarized light-out configuration. T-MSHG has much larger contrast ratio than T-MOKE.

The hysteresis loops for SP-enhanced T-MSHG and T-MOKE and the contrast ratios based on the hysteresis loops are shown in Fig. 3. Both show an increased contrast ratio as total reflection becomes more attenuated. However, the contrast ratio of enhanced T-MSHG is more than one order of magnitude larger than the T-MOKE. The combination of large magnetic contrast, highly enhanced T-MSHG and the high surface sensitivity of SPs shows great potential for a new generation of nonlinear magneto-optical SPs sensor for bio-chemical applications.

#197522 - $15.00 USD Received 17 Sep 2013; revised 8 Oct 2013; accepted 8 Oct 2013; published 15 Nov 2013

4. Discussion

The SPP-enhanced SHG originates from the metal/air interface [1–3, 22]. Here, the iron side of the iron/air interface is the source of MSHG under ATR condition. Simon et al. show that under ATR condition, SHG at the metal/air interface is much greater than that at the substrate/metal interface [2], and Tsang points out that the interference between the two contributions makes up the noise-like background in the vicinity of ATR [22]. In our measurement [Fig. 2(b)] the SHG signal without ATR is very small, so that SHG at the substrate/metal interface is not considered in our simulation. According to the surface-plasmon field-enhancement theory, the value of the field enhancement is given by the ratio of the field intensity (light intensity) on the metal surface (the metal/air interface) divided by the incoming field intensity in the prism (substrate/metal interface) [1]. Hence, the enhancement of SHG can be defined as the square of the field enhancement. Since only the relative intensity and trends of SHG are simulated here, the propagation of the SHG beam is not being considered in the model. In the simulation, the refractive index of prism is 1.5, the refractive index of MgO is 1.73 and $\varepsilon_{iron} = -4.5 + 22i$ [23]. This model agrees with our experimental data [Fig. 2(a)] on sample I very well [Fig. 4(a)], because it has been demonstrated that the SHG signal comes from the metal/air surface and it is a non-magnetic process in this case. However, when taking into account the magnetic contribution, it becomes more complex and there is a big difference between experimental T-MSHG data for sample II [Fig. 2(b)] and the simulated SHG values [Fig. 4(b)], although the experimental and simulated ATR curves are almost identical. The experimental data stretch out and keep a high intensity as the incident angle increases, while the calculated SHG intensity drops very fast. Here the trends of field intensity in each direction (x and z) need to be considered.

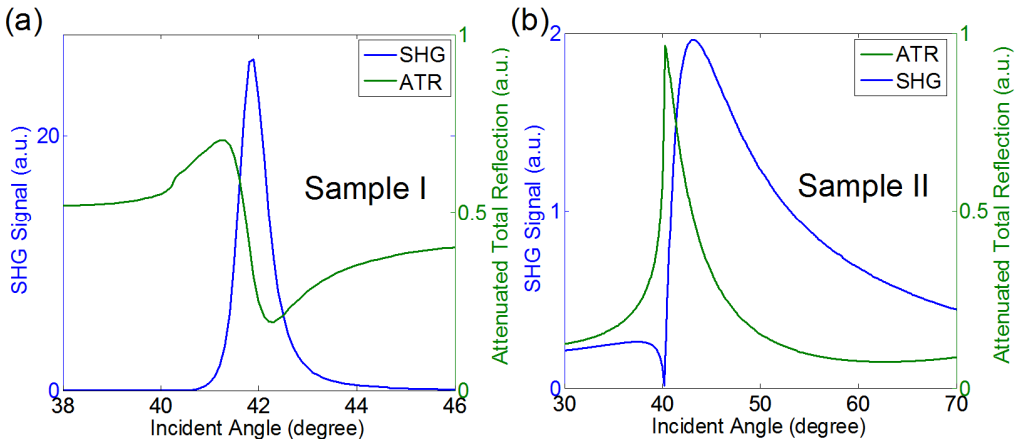

Fig. 4. Simulated ATR and SHG for sample I (a) and II (b).

The strength of incident P-polarized light at the prism/iron interface can be decomposed into two components $Ez_0 = E_0 \sin\theta'$ and $Ex_0 = E_0 \cos\theta'$, where θ' is the incident angle at that interface. After the SPs field-enhancement factor is also considered, Ez and Ex at the iron/air interface can be calculated and are displayed in Fig. 5(a), showing different trends as the incident angle increases. It has been demonstrated that the second-order surface susceptibility tensor components in the x-direction (χ_{xxx}, χ_{xzx} and χ_{xzz}) contribute most to the second-harmonic generation [2,3,11] because the generation of a surface wave at the SHG frequency is a fully surface specific process. As a result, the intensity of T-MSHG can be simplified as:

$$I^{T-MSHG}(+M) = \varepsilon_0^2 \cdot \left(\chi_{xxx}^{odd} \cdot E_x^2 + \chi_{xzz}^{odd} \cdot E_z^2 + \chi_{xzx}^{even} \cdot 2E_z E_x\right)^2 \qquad (6)$$

#197522 - $15.00 USD Received 17 Sep 2013; revised 8 Oct 2013; accepted 8 Oct 2013; published 15 Nov 2013

$$\text{and} \quad I^{T-MSHG}(-M) = \varepsilon_0^2 \cdot \left(-\chi_{xxx}^{odd} \cdot E_x^2 - \chi_{xzz}^{odd} \cdot E_z^2 + \chi_{xzx}^{even} \cdot 2E_z E_x\right)^2, \qquad (7)$$

depending on the direction of M. From this expression, we notice that the trend of T-MSHG intensity as a function of incident angle will be affected largely by the weight of E_x^2 and E_z^2. In other words, knowing the trends of E_x and E_z as a function of incident angle [Fig. 5(a)], we can calculate the intensity of T-MSHG, if we know the relative value of χ_{xxx}^{odd} and χ_{xzz}^{odd}.

We found that if χ_{xxx}^{odd} dominates, the T-MSHG intensity exhibits a very steep drop with increasing angle-of-incidence [Fig. 5(b), Set 2], while if χ_{xzz}^{odd} dominates, T-MSHG remains a high value for large incident angles [Fig. 5(b) set 1]. The latter one agrees with our experimental data [Fig. 2(b)] very well. Hence, there exists a great anisotropy in the second-order susceptibility tensor of T-MSHG.

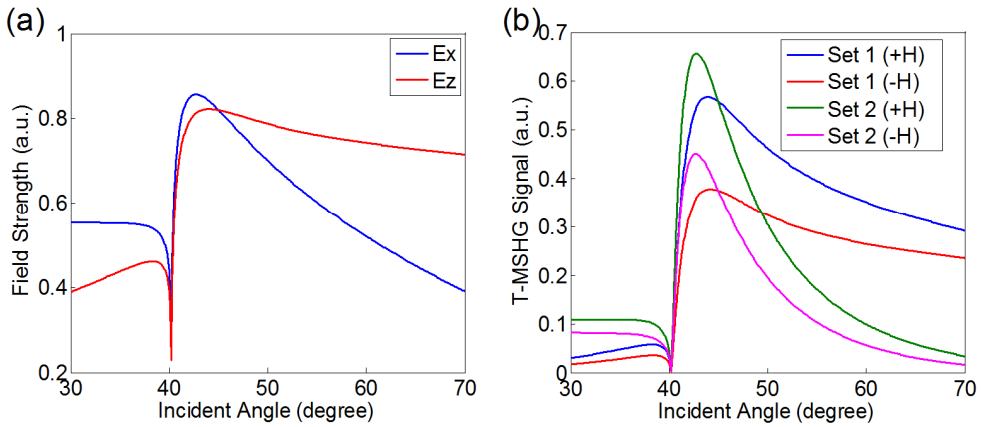

Fig. 5. (a) Field strength of Ex and Ez, (b) Simulated T-MSHG signal. Set 1: χ_{xxx}^{odd} / χ_{xzz}^{odd} = 1:100, Set 2: χ_{xxx}^{odd} / χ_{xzz}^{odd} = 100:1.

5. Conclusion

In this work, we combined two surface sensitive effects, magnetic second-harmonic generation and surface plasmons, to directly study the interaction between MSHG and SPs. Enhanced T-MSHG and magnetic contrast ratio are achieved, which has potential for the development of a new generation of bio-chemical sensors. We also demonstrate that for the single-crystal iron film surface, χ_{xzz}^{odd} dominates the nonlinear susceptibility tensor. In other words, the expression of transverse MSHG can be simplified as

$$I^{T-MSHG}(\pm M) = \varepsilon_0^2 \cdot \left(\pm\chi_{xzz}^{odd} \cdot E_z^2 + \chi_{xzx}^{even} \cdot 2E_z E_x\right)^2. \qquad (8)$$

Acknowledgments

The optical experiments performed at the College of William and Mary are supported by the Department of Energy through Grant No. DE-FG02-04ER46127. The sample growth at NRL is supported by core programs and the Office of Naval Research.

#197522 - $15.00 USD Received 17 Sep 2013; revised 8 Oct 2013; accepted 8 Oct 2013; published 15 Nov 2013